CRYSTAL GROWTH & DESIGN

Article

pubs.acs.org/crystal

Exploring Supramolecular Self-Assembly of Tetraarylporphyrins by Halogen Interactions. 3. Tin(L)$_2$(A_2B_2-Porphyrin) Arrays Supported by Concerted Halogen and Hydrogen Bonding

Hatem M. Titi, Goutam Nandi, Bharat Kumar Tripuramallu, and Israel Goldberg*

School of Chemistry, Sackler Faculty of Exact Sciences, Tel-Aviv University, Ramat-Aviv, 69978 Tel-Aviv, Israel

Supporting Information

ABSTRACT: This work reports on a designed construction of new porphyrin-based supramolecular architectures assembled with the aid of halogen bonds and a combination of halogen and hydrogen bonding interactions. The tin^{IV}(L)$_2$-tetraarylporphyrin building unit (L = axial ligand) was used to this end, wherein suitable donor and acceptor functions for such bonds have been introduced in a complementary manner on the axial ligands and the porphyrin periphery. We reveal in this context eight structures involving differently substituted metalloporphyrin entities: 5,10,15,20-tetra(4′-iodophenyl)porphyrin (A_4-P), 5,10,15,20-tetra-(4′-pyridyl)porphyrin (B_4-P), 5-(4′-pyridyl)-10,15,20-tris(4′-iodophenyl)porphyrin (A_3B-P), and 5,15-bis(4′-pyridyl)-10,20-bis(4′-iodophenyl)porphyrin (A_2B_2-P), and various axial ligands attached to the tin center and bearing molecular recognition capacity. The latter include 3-hydroxypyridine (L1), hydroxyl (L2), 1-hydroxybenzotriazole (L3), 5-bromopyridine-3-carboxylic acid (L4), 5-bromoisophthalic acid (L5), 5-hydroxyisophthalic acid (L6), and 2,5-thiophenedicarboxylic acid (L7). The various porphyrin-Sn(L)$_2$ combinations that could be obtained in a single-crystal form were structurally analyzed by single-crystal X-ray diffraction, and their intermolecular interaction patterns were rationalized by computational methods. The versatile (A_2B_2-P) system deserved the most attention, and the crystal structure of this free-base porphyrin was determined as well. The occurrence of supramolecular halogen interactions between neighboring porphyrin moieties, as structure directing agents, was successfully manifested in our systems. Other findings of particular interest are that the assembly of [Sn(3-hydroxypyridine)$_2$(A_4-P)] (compound **1**) displays a short intermolecular I···O halogen interaction at 2.949 Å, facilitated by a self-activation process through concomitant involvement of the iodine substituents in I···I contacts. Compound **2** [{Zn(A_4-P)}$_2$Sn(OH)$_2$(B_4-P)] illustrates the first porphyrinic trimer assembly driven by halogen bonding interactions. Then, compounds **6** [Sn(5-bromoiso-phthalate)$_2$(A_2B_2-P)·(PhNO$_2$)], **7** [Sn(5-bromo-isophthalate)$_2$(A_2B_2-P)·(DMF)], **8** [Sn(5-hydroxyisophthalate)$_2$(A_2B_2-P)], and **9** [Sn(2,5-thiophene-dicarboxylate)$_2$(A_2B_2-P)·(PhNO$_2$)$_3$] reveal strong halogen interactions alongside tight hydrogen bonding contacts. In **9** the relatively rare I···S halogen bonding has been detected in porphyrin assemblies for the first time.

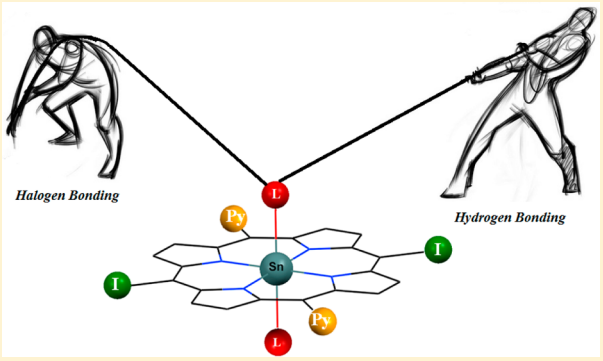

INTRODUCTION

Halogen bonding (XB) is an excellent tailoring tool for the rational design of attractive supramolecular assemblies.[1−3] This interaction is characterized by strong directionality, occurring between the partially positive electrostatic potential of the polarized halogen atom X, at the tip of e.g., a C−X bond, known as a σ-hole (halogen bond acceptor), and the electron-rich Lewis base atoms in the nearest environment bearing lone electron pairs such as N, O, S, I, or Br (halogen bond donors).[4] Direct halogen−halogen interactions can be divided into two main types (from the electron-donor electron-acceptor perspective; Scheme 1). Type I occurs between two polarized halogen atoms, where the σ-hole of one of them is partially overlapped by the negative equatorial belt region of the second halogen. The optimal geometry of the C−X···X−C interaction is characterized by $\theta_1 = \theta_2$ (Scheme 1). Type II occurs when the two halogen atoms are orthogonal to each other, where $\theta_1 \approx 90°$ and $\theta_2 \approx 180°$. When the electron donor is a non-halogen atom such as nitrogen, the directional interaction σ-hole−electron pair can be categorized as type II, where the optimal angle is $\theta = 180°$ (Scheme 1).[5] There has been a growing interest in utilizing halogen bonds, due to their directional nature and significant strength, in diverse applications such as supramolecular liquid crystals,[6−8] nonlinear optical responses,[9−11] gel formation,[12] drug design,[13] catalytic systems,[14,15] anion sensing,[16] and in crystal engineering.[17]

Investigating supramolecular self-assembly of the tetraarylporphyrin compounds (TArP) by halogen bonding offers a great challenge in crystal engineering. Porphyrins are interesting in materials chemistry owing to their various

Received: April 19, 2015
Revised: May 8, 2015
Published: May 8, 2015

DOI: 10.1021/acs.cgd.5b00543
Cryst. Growth Des. 2015, 15, 3063−3075

Scheme 1. Schematic representation of Type I and Type II Halogen Bonds, Where the Electron-Deficient Zone of the Polarized Halogen Atom X (Depicted by $+\delta$) Interacts with an Electron-Rich Zone of Another Halogen (Depicted by $-\delta$) or with an Electron Donor with Exposed Lone Electron Pairs (e.g., D = N, O, or S)

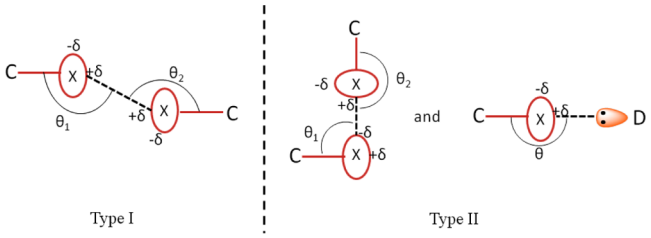

applications in photochemistry, catalysis, and electronic properties.[18−20] More importantly, crystal engineering with aryl porphyrins and their metalated derivatives has led to many attractive crystalline architectures, due to minimal flexibility of their molecular backbone and multiple sites for potential functionalization.[21−23] Others and we have demonstrated the self-assembly of various tetra(iodophenyl)porphyrin (TIPP) derivatives through diverse methodologies.[24−27] Recently, we have chosen a six-coordinate tin-porphyrin scaffold as the main building block for the self-assembly process. The preferred 4+ oxidation state of the tin metal ion and its strong oxophility facilitate the association of two monoanionic axial ligands (as RO^- or $RCOO^-$) to the tin center. Substitution of additional functional groups (of Lewis base nature) on these ligands as halogen, N, O, or S is required to invoke effective multiple halogen bonding with the periphery of neighboring porphyrin moieties. A similarly rationalized approach can be used with other metal ions in the porphyrin center, and diversified substitution of halogen bond donor and acceptor functions on the porphyrin core. In this manner porphyrin scaffolds with different metal centers, bearing various functional groups on their periphery and on the axial ligands, have led to the formation of interesting supramolecular assemblies directed by I···N and I···O halogen interactions.[26,28−30] It has been shown that such metalloporphyrin model systems can be efficient also in assembling arrays by hydrogen bonds, an appropriate example involving the six-coordinate tin-tetra(pyridyl)-porphyrin framework with axial ligands decorated with carboxylic acid groups.[31]

The present work demonstrates further successful efforts to utilize the halogen and hydrogen bonding molecular recognition features, also in concert, in our crystal engineering efforts of new porphyrinic supramolecular assemblies. To this end we have synthesized a series of diversely functionalized six-coordinate tin-porphyrin derivatives that incorporate in a complementary manner donor and acceptor molecular recognition functions for halogen bonding and a possible combination of hydrogen and halogen interactions (our earlier reports addressed separately the assembly of such porphyrin complexes either by hydrogen bonds[31] or by halogen bonds[25]). The various porphyrin scaffolds and axial ligands used in the present work are illustrated in Scheme 2. The former are of the A_4-P, B_4-P, A_3B-P, and A_2B_2-P types (where A and B represent different aryl substituents; 4-iodophenyl and 4-pyridyl, respectively), while the axial ligands bound to the tin center contain additional molecular recognition functionalities (N, O, S, and COOH) for halogen and hydrogen bonding. We

Scheme 2. Schematic Demonstration of the Molecular Components Involved in This Study[a]

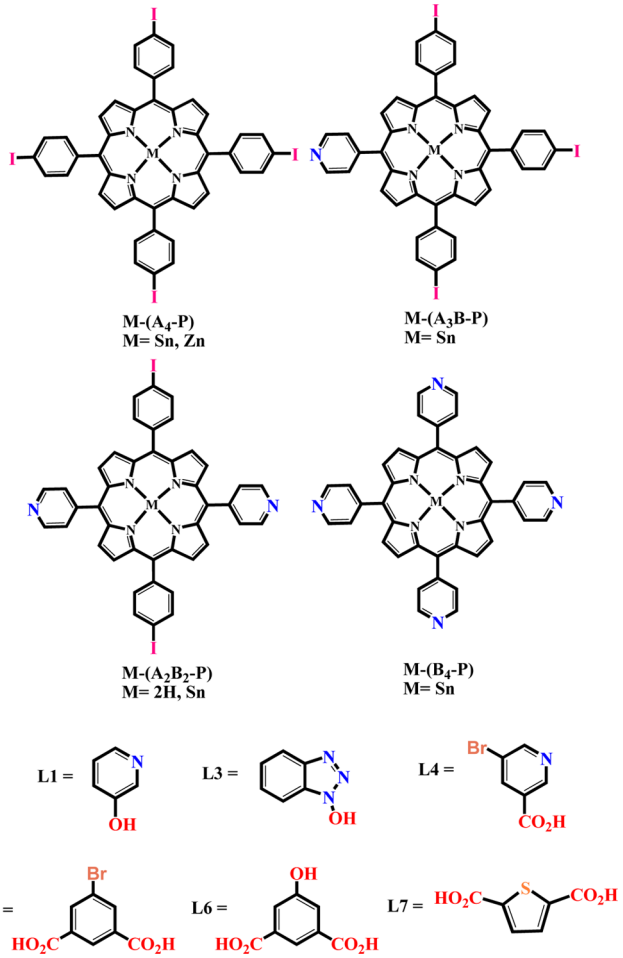

[a]In the porphyrin moieties (two top rows), A refers to the iodophenyl and B to the pyridyl substituents; the corresponding ligands are 5,15-bis(4′-pyridyl)-10,20-bis(4′-iodophenyl)-porphyrin (A_2B_2-P), 5-(4′-pyridyl)-10,15,20-tris(4′-iodophenyl)porphyrin (A_3B-P), 5,10,15,20-tetra(4′-iodophenyl)-porphyrin (A_4-P), 5,10,15,20-tetra(4′-pyridyl)-porphyrin (B_4-P). The axial ligands (bottom two rows) consist: 3-hydroxypyridine (L1), hydroxyl (L2), 1-hydroxybenzotriazole (L3), 5-bromopyridine-3-carboxylic acid (L4), 5-bromoisophthalic acid (L5), 5-hydroxyisophthalic acid (L6), and 2,5-thiophenedicarboxylic acid (L7).

describe herein the self-assembled architectures of the following compounds (oftentimes crystallized as solvates with either ordered or disordered molecules of the lattice-included solvent): $[Sn(L1)_2(A_4\text{-P})]$ (**1**), $[\{Zn(A_4\text{-P})\}_2Sn(L2)_2(B_4\text{-P})]$ (**2**), $[Sn(L3)_2(A_3B\text{-P})\cdot(DMF)\cdot(H_2O)]$ (**3**), $[A_2B_2\text{-P}]$ (**4**), $[Sn(L4)_2(A_2B_2\text{-P}]$ (**5**), $[Sn(L5)_2(A_2B_2\text{-P})\cdot(PhNO_2)]$ (**6**), $[Sn(L5)_2(A_2B_2\text{-P})\cdot(DMF)]$ (**7**), $[Sn(L6)_2(A_2B_2\text{-P})]$ (**8**), and $[Sn(L7)_2(A_2B_2\text{-P})\cdot(PhNO_2)_3]$ (**9**). Intermolecular halogen bonding is well manifested in structures **1**−**9**. Compound **2** is a unique example of porphyrin coordination trimers assembled by halogen bonds. Arrays of complexes **6**−**9** exhibit a concerted utilization of hydrogen as well as halogen bonding in the self-assembly process. Table 1 summarizes the main noncovalent interactions that occur in the crystal structures of the various compounds.

DOI: 10.1021/acs.cgd.5b00543
Cryst. Growth Des. 2015, 15, 3063−3075

Table 1. Illustration of the Prominent Hydrogen Bonding (HB) and Halogen Bonding (XB) Interactions in Structures of 1−9[a]

complex	HB (Å)	XB (Å)	XB type
1		2.947(5)	I···O
2		3.193(10)	I···N
3		3.031(6)	I···N
4		3.378(5)	I···N
5		3.040(6)	I···N
6	OH···N = 2.592(5)	3.015(5)	I···O
7	NH···O = 2.648(9)	3.259(9)	I···O
8	OH···N = 2.640(6)	3.104(6)	I···O
9	OH···N = 2.646(5)	3.437(5)	I···S

[a]The listed distances are considerably shorter (in most cases) than the sum of the corresponding van der Waals radii (r_{vdW} for I, S, N, and O taken as 2.10, 1.85, 1.50, and 1.40 Å, respectively; Gavezzotti, 1983).[44]

EXPERIMENTAL SECTION

In all the reactions commercially available reagents of analytical grade were used without further purification. IR spectra were recorded on a Bruker Tensor 27 system spectrophotometer in ATR mode. The metalation of the various porphyrin materials of types A_4-P B_4-P and A_3B-P (A = iodophenyl and B = pyridyl groups) was carried out as described in our previous reports and illustrated in Scheme 3.[25,29,31] The modified synthesis of the A_2B_2-P compound,[32] its metalation, and preparation of complexes **1**−**9** are detailed below.

Scheme 3. Synthetic Routes for the Various Porphyrin Scaffolds Used in the Present Study

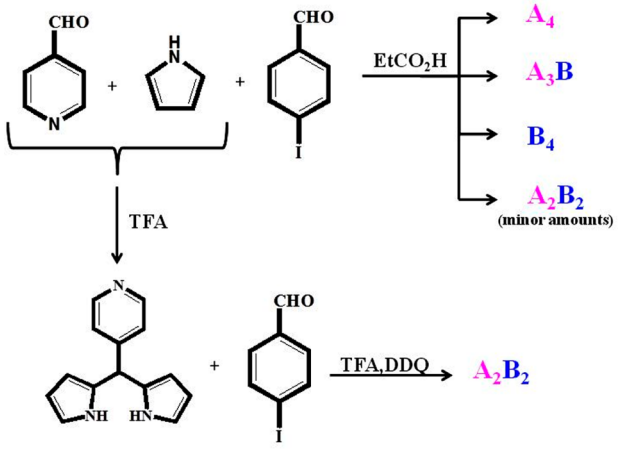

5-(4-Pyridyl)dipyrromethane was prepared as described in the literature.[32]

5,15-Bis(4′-pyridyl)-10,20-bis(4′-iodophenyl)-porphyrin (H_2-A_2B_2-P). 5-(4-Pyridyl)dipyrromethane (0.250 g, 1.12 mmol) and 4-iodobenzaldehyde (0.183 g, 1.12 mmol) were dissolved in 350 mL of anhydrous dichloromethane (DCM) under Ar. The mixture was cooled at 0 °C in an ice bath, trifluoroacetic acid (TFA) was added (dropwise) (3.56 mL, 48.2 mmol), and the mixture was stirred for 20 min at 0 °C. DDQ (0.500 g, 2.24 mmol) was then added, and the reaction mixture was stirred at room temperature for 1 h. The organic phase was washed with saturated $NaHCO_3$ and water, and dried over anhydrous Na_2SO_4 and the solvent was removed. Purification by column chromatography (on alumina, with 5% acetone in chloroform eluent) afforded a purple solid. Yield 32%. ^{1}H NMR (400 MHz, δ-$CDCl_3$): 7.93 (d, 4H), 8.10 (d, 4H), 8.16 (d, 4H), 8.81 (d, 4H), 8.88 (d, 4H), 9.05 (dd, 4H).

Synthesis of [Sn(OH)$_2$-(A_2B_2-P)]. In the first stage the dichloro-tin derivative was prepared.[31] A mixture of H_2-A_2B_2 (100 mg, 0.09 mmol) and $SnCl_2{\cdot}2H_2O$ (67 mg, 0.3 mmol) was dissolved in 30 mL of pyridine; then it was refluxed on an oil bath overnight and evaporated to dryness. The residual was dissolved in 100 mL of chloroform and washed with distilled water twice. The water was removed and the oil layer was dried with Na_2SO_4. The mixture was concentrated and purified by chromatography using aluminum oxide column with a 2:98 methanol/chloroform mixture. Yield: 70%. In the second step, the dichloride was converted to the dihydroxide derivative by reacting 70 mg (0.05 mmol) of $Sn(A_2B_2)(Cl)_2$ dissolved in 50 mL of chloroform with 1 mmol of NaOH dissolved in 10 mL of water. The mixture was stirred overnight at room temperature and then washed several times with distilled water. After drying with Na_2SO_4, most of the chloroform was removed, and the remaining product was purified by chromatography using aluminum oxide with 2:98 methanol/chloroform mixture. Yield: 88%. IR (cm^{-1}): 1655, 1592, 1468, 1406, 1346, 1210, 1072, 1060, 1024, 1004, 888, 850, 793, 718, 660, 544, 523, 457.

Compound 1. A mixture of Sn(OH)$_2$-(A_4-P) (3 mg, 0.002 mmol) and 3-hydroxypyridine (3 mg, 0.033 mmol) as axial ligand was dissolved in 400 μL of DMF, and the reaction mixture was heated in bath reactor at 100 °C for 1 h. Then 3 mg (0.027 mmol) of 1,4-diazabicyclo-[2,2,2]-octane was added and the mixture was heated for further 24 h. After the mixture was cooled, an additional 1 mL of chloroform was added. The resulting crystals were obtained after a few days by slow evaporation. IR (cm^{-1}): 1652, 1573, 1470, 1386, 1314, 1276, 1210, 1143, 1060, 1027, 1002, 796, 749, 707, 601, 563.

Compound 2. The trimeric porphyrin of **2** was synthesized by dissolving Sn(OH)$_2$-(B_4-P) (3 mg, 0.004 mmol) and Zn-(A_4-P) (4.5 mg, 0.004 mmol) in dimethylacetamide (DMA). The mixture was heated in bath reactor for 100 °C for 2 days, and then it was cooled slowly to room temperature. It was left for slow evaporation for a week. Purple crystals were obtained. IR (cm^{-1}): 3402, 2935, 1715, 1609, 1494, 1382, 1259, 1188, 1054, 1013, 988, 846, 783, 741, 700, 590, 555.

Compound 3. A mixture of Sn(OH)$_2$-(A_3B-P) (2 mg, 0.002 mmol) and 1-hydroxybenzotriazole (3 mg, 0.022 mmol) was dissolved in 2 mL of DMF. The resulting solution was heated for 1 h at 100 °C in bath reactor. After cooling, additional two drops of nitrobenzene and 2 mL of chloroform were added to the reaction vial, and the mixture was left for slow evaporation at ambient conditions. X-ray quality crystals of compound **3** were obtained after 2 weeks. IR (cm^{-1}): 3415, 2932, 1649, 1494, 1439, 1412, 1388, 1348, 1255, 1097, 1062, 865, 851, 799, 745, 710, 660.

Compound 4. Crystals of the free-base porphyrin were obtained unintentionally by mixing Sn(OH)$_2$-(A_2B_2-P) (2 mg, 0.002 mmol) and 5-aminoisophthalic acid (3 mg, 0.017 mmol). These reagents were dissolved in a 1 mL mixture of DMF, and the solution was heated for 1 h at 100 °C. After cooling, two drops of $PhNO_2$ and 1 mL of chloroform were added, and the solution was left for slow evaporation. After 2 weeks, reddish crystals of A_2B_2-P (but not of the anticipated tin complex) were obtained. IR (cm^{-1}): 2923, 2854, 1674, 1548, 1478, 1345, 1257, 1092, 851, 793, 703, 679.

Compound 5. Sn(OH)$_2$-(A_2B_2-P) (2 mg, 0.002 mmol) was dissolved in 2 mL of DMF:EtOH followed by the addition of 5-bromopyridine-3-carboxylic acid (6 mg, 0.029 mmol). The mixture was transferred to a sealed vial and heated for 2 days at 100 °C in bath reactor. Later, the reaction was cooled and allowed to slowly evaporate at ambient conditions. X-ray quality crystals of **5** were obtained after 1 week. IR (cm^{-1}): 3415, 2933, 1650, 1494, 1439, 1412, 1388, 1254, 1098, 1062, 865, 793, 731, 660.

Compound 6. Single crystals of **6** were obtained by dissolving Sn(OH)$_2$-(A_2B_2-P) (2 mg, 0.002 mmol) and 5-bromoisophthalic acid (3 mg, 0.012 mmol) in 600 μL of a 1:2 DMF:$PhNO_2$ mixture. The resulting solution was sealed and heated for 2 days at 100 °C in a bath-reactor. Dark-red crystals of the corresponding complex were obtained (as nitrobenzene solvate) after cooling the reaction mixture to ambient conditions. IR (cm^{-1}): 1519, 1478, 1344, 1315, 1068, 1020, 933, 850, 792, 701, 678.

Compound 7. A slight modification of the crystallization environment led to another solvate of the tin-porphyrin−bromoisophthalic acid complex. This procedure involved mixing Sn(OH)$_2$-(A_2B_2-

DOI: 10.1021/acs.cgd.5b00543
Cryst. Growth Des. 2015, 15, 3063−3075

Table 2. Crystal Data and Structure Refinement Summary for Complexes 1−9[a]

compound	1	2	3	4	5
chemical formula	$C_{54}H_{32}N_6O_2I_4Sn$	$C_{128}H_{74}N_{16}O_2I_8SnZn_2$	$2(C_{55}H_{32}N_{11}O_2I_3Sn)\cdot2(C_3H_7NO)\cdot H_2O$	$C_{42}H_{24}N_6I_2$	$C_{54}H_{30}N_8O_4Br_2I_2Sn$
formula weight	1423.14	3132.69	2920.83	866.47	1387.17
crystal system	monoclinic	triclinic	monoclinic	monoclinic	triclinic
space group	$C2/c$	$P\bar{1}$	$P2/c$	$P2_1/n$	$P\bar{1}$
T/K	110	110	110	110	110
a/Å	26.1417(6)	12.5951(7)	29.1636(8)	6.3885(3)	10.4991(7)
b/Å	9.2708(2)	14.0035(10)	9.5465(3)	22.325(2)	12.9238(7)
c/Å	25.2635(6)	25.5337(19)	21.3518(6)	28.971(2)	20.5966(14)
α/°	90	77.984(4)	90	90	100.132(3)
β/°	107.854(1)	83.401(3)	100.586(2)	91.980(2)	104.578(3)
γ/°	90	73.505(3)	90	90	100.979(2)
Z	4	1	2	4	2
V/Å^3	5827.9(2)	4216.1(5)	5843.4(3)	4129.4(5)	2580.5(3)
D_{calc}/g·cm^{-3}	1.622	1.234	1.660	1.394	1.785
μ/mm^{-1}	2.598	1.935	2.077	1.557	3.294
reflections collected	21086	56777	54225	29332	31101
$2\theta_{max}$/°	56.6	51.0	56.6	50.12	50.18
unique reflections	7257	15491	11265	7317	9102
R_{int}	0.029	0.039	0.048	0.061	0.032
R_1/wR_2 [$I > 2\sigma(I)$]	0.039/0.102	0.075/0.188	0.061/0.135	0.041/0.086	0.067/0.189
R_1/wR_2 (all data)	0.048/0.106	0.118/0.201	0.091/0.141	0.065/0.091	0.081/0.198
goodness-of-fit	1.067	1.079	1.093	0.993	1.047

compound	6	7	8	9
chemical formula	$C_{70}H_{42}N_8O_{12}Br_2I_2Sn$	$C_{58}H_{32}N_6O_8Br_2I_2Sn\cdot2(C_3H_7NO)$	$C_{58}H_{34}N_6O_{10}I_2Sn$	$C_{54}H_{30}N_6O_8S_2I_2Sn\cdot3(C_6H_5NO_2)$
formula weight	1719.42	1619.40	1347.40	1695.77
crystal system	triclinic	triclinic	triclinic	triclinic
space group	$P\bar{1}$	$P\bar{1}$	$P\bar{1}$	$P\bar{1}$
T/K	110	110	110	110
a/Å	11.2642(7)	9.1280(6)	9.5779(7)	9.0924(3)
b/Å	12.6141(7)	12.0763(7)	12.8239(10)	13.8395(5)
c/Å	13.3936(8)	14.3062(9)	13.6142(12)	15.4844(7)
α/°	80.256(3)	95.817(2)	81.994(3)	76.065(2)
β/°	79.612(3)	93.651(2)	87.205(3)	82.580(3)
γ/°	67.802(2)	95.135(2)	88.339(3)	72.433(1)
Z	1	1	1	1
V/Å^3	1722.4(2)	1558.4(2)	1653.5(2)	1799.6(1)
D_{calc}/g·cm^{-3}	1.658	1.726	1.353	1.565
μ/mm^{-1}	2.493	2.748	1.373	1.340
reflections collected	30644	38872	14611	23002
$2\theta_{max}$	56.74	50.11	50.25	50.18
unique reflections	8488	5499	5803	6366
R_{int}	0.032	0.060	0.040	0.031
R_1/wR_2 [$I > 2\sigma(I)$]	0.054/0.139	0.066/0.141	0.054/0.144	0.051/0.124
R_1/wR_2 (all data)	0.069/0.146	0.105/0.165	0.079/0.152	0.061/0.129
goodness-of-fit	1.024	1.079	1.099	1.078

[a]With the exception of compound 7, the data in this table relate to refined structural models that exclude some severely disordered molecules of the crystallization solvent.

P) (2 mg, 0.002 mmol) and 5-bromoisophthalic acid (3 mg, 0.012 mmol) in 2 mL of a 1:2 DMF/ethanol solution. The dissolved compounds were heated in a bath reactor for 2 days at 100 °C; after cooling, the mixture was left for slow evaporation to form reddish crystals (of the same complex as in **6**, but as a DMF solvate) after 3 days. IR (cm^{-1}): 3415, 2933, 1649, 1494, 1439, 1412, 1388, 1254, 1097, 1062,865, 800, 760, 659.

Compound 8. **8** was obtained by mixing $Sn(OH)_2$-(A_2B_2-P) (2 mg, 0.002 mmol) and 5-hydroxyisophthalic acid (3 mg, 0.016 mmol) in 600 μL of 1:2 DMF/$PhNO_2$. This reaction mixture was heated in a bath reactor for 38 h at 100 °C, then cooled slowly to room temperature, and left for slow evaporation for a few days, yielding X-ray quality crystals. IR (cm^{-1}): 1669, 1519, 1478, 1386, 1344, 1255, 1091, 1069, 1003, 935, 851, 794, 702, 678, 659.

Compound 9. **9** was obtained by mixing $Sn(OH)_2$-(A_2B_2-P) (2 mg, 0.002 mmol) and 2,5-thiophenedicarboxylic acid (3 mg, 0.017 mmol) in 600 μL of 1:2 DMF/$PhNO_2$. The resulting mixture was sealed and heated in bath reactor for 2 days at 100 °C, followed by slow cooling to room temperature. The reaction mixture was left for slow evaporation for 4 days, yielding good crystals for crystallographic evaluation. IR (cm^{-1}): 1677, 1604, 1519, 1477, 1343, 1316, 1259, 1107, 1068, 1021, 1004, 934, 850, 792, 700, 676.

Crystal Structure Determinations. The X-ray measurements [Bruker-ApexDuo diffractometer, IμS microfocus MoKα radiation] were carried out at ca. 110(2) K on crystals coated with a thin layer of

DOI: 10.1021/acs.cgd.5b00543
Cryst. Growth Des. 2015, 15, 3063−3075

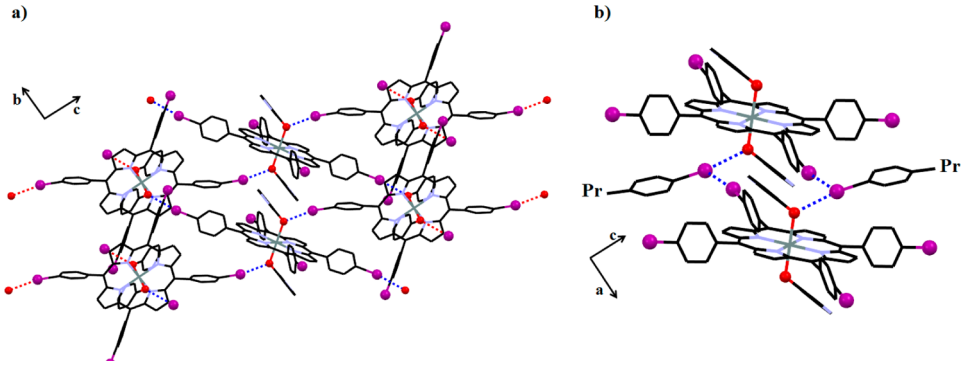

Figure 1. (a) 2D Halogen-bonded arrays in the crystal structure of **1**, where the O-sites (red spheres) are involved in directional interactions with the I atoms (violet large spheres) of neighboring molecules. (b) Schematic representation of the halogen interactions (blue dashed lines) between different layers. "Pr" represents the remaining part of the porphyrin entity.

amorphous oil to minimize crystal deterioration, possible structural disorder, and related thermal motion effects, and to optimize the precision of the structural results. These structures were solved by direct and Fourier methods and refined by full-matrix least-squares (using standard crystallographic software (SHELXTL-2014, SHELXL-2014)).[33,34] Most compounds (with the exception of **7** were found to contain molecules of either partly and/or severely disordered crystallization solvent (DMF, DMA, and ethanol). The contribution to the diffraction pattern of the disordered moieties that could not be reliably modeled by discrete atoms was subtracted by the SQUEEZE procedure, using the PLATON software.[35] In some compounds the iodo/bromo-phenyl groups exhibit orientation disorder as well, best manifested by split positions of the aryl ring or the terminal I/Br atoms. This had little effect, however, on the precision of the structure determination of the porphyrin assembly modes and of the interaction distances relevant to the present discussion. The integrity of the crystalline samples was confirmed by matching between the simulated and the experimental powder X-ray diffraction patterns. The crystallographic and experimental data for **1**−**9** are given in Table 2. CCDC nos. are 1059756−1059764.

RESULTS AND DISCUSSION

As indicated at the outset, the main purpose of this study was to involve halogen interactions in the assembly process of porphyrin-based supramolecular arrays. The tin-porphyrin complexes were targeted, accordingly, to bear simultaneously both halogen bond donor (halogen, N, O, and S atoms containing lone electron pairs) and acceptor (polarizable iodine substituents) functionalities on the molecular backbone. In the last part of this study the molecular building units were decorated with additional hydrogen bond donor and acceptor functions in order to allow concomitant intermolecular association via hydrogen bonds as well.

The first example expands on our earlier findings on I···O halogen bonded porphyrin arrays.[26] Compound **1** involves a six-coordinate tin−tetra(4′-iodophenyl)porphyrin with two axial ligands of 3-hydroxypyridine bound (through O^-) to the tin center from both sides of the porphyrin plane. The analysis of its crystal structure reveals the presence of halogen bonded 2D sheets of the molecular units, which are aligned roughly parallel to the *bc* plane of the crystal (Figure 1a). Two of the peripheral I atoms of the 4-iodophenyl arms at the *meso*-positions of the porphyrin macrocycle were found to be directionally involved in halogen interactions with the O-sites of the axial ligands. Every porphyrin complex is linked to four different neighboring units via I···O interactions between the iodine atoms of the porphyrin periphery and the O-sites of the axial ligands. The observed I···O intermolecular interaction distance of 2.947 Å is about 16% shorter than the sum of the corresponding van der Waals radii of I and O. The Sn−O···I angle is 122.4°, indicating that one of lone electron pairs of O is directed at the electron-deficient σ-hole at the tip of the C−I bond, providing attractive contribution to this interaction. Only a small number of similar iodine-to-oxygen interactions in porphyrin assemblies have been reported by us, but with longer I···O intermolecular bonds of, e.g., 2.998 Å[28] and 3.298 Å.[26] In **1** the 2D supramolecular layers exhibit additional relatively strong type-II I···I contacts of 3.74 Å (which is shorter by about 0.46 Å than the sum of the van der Waals radii of covalently bound I). These halogen interactions contribute further to the polarization of the electron density around (and to deepening the σ-hole of) the iodine atom that interacts with O, and the enhancement of their Coulombic attraction to the electron-rich O-site. The electron density of the latter, being located above and below the porphyrin center, is intensified additionally by the porphyrin ring current, as confirmed by earlier calculations of the electrostatic potential distribution around similar porphyrin entities.[25] The above reasoning may explain the relatively short I···O interaction in the present case (see below). Figure 1b illustrates the halogen bonding pattern in **1**.

A survey of the Cambridge Structural Database (ConQuest Version 1.17, 2014) reveals 69 crystal structures with prominent I···O interactions between an Ar−O−Y halogen bond donor (Ar represents an aromatic ring and Y any atom) and an Ar−I halogen bond acceptor. The search was limited to structures in which the distance between the I-sites and the O atoms is shorter than the sum of the corresponding van der Waals radii (3.5 Å). A histogram of structures in this specific category (Figure 2) shows that the halogen bond observed in **1** (2.947 Å) falls among the three shortest interactions. In the structure exhibiting the shortest I···O contact (2.898 Å; Refcode ISIJAV) the I-halogen-bond-acceptor site of the 3,6-diiodo-tetrafluorobenzene fragment is "activated" by the electron-withdrawing F-substituents that deepen the σ-hole on I. It can be argued that the relatively strong I···O interaction in **1** is similarly "activated" by the simultaneous involvement of the relevant iodine substituent in I···I contacts (see above).

It might be of interest to compare the halogen bonding scheme observed in **1** with that found in its previously reported pseudopolymorph (different solvate, Refcode HIRWEM).[25] In the latter, the I-sites of the porphyrin component are involved preferably in weak I···$N_{pyridyl}$ interactions (at 3.122 Å) to the 3-hydroxypyridyl axial ligands (rather than in I···O contacts as in **1**). In order to rationalize these empirical observations, we

DOI: 10.1021/acs.cgd.5b00543
Cryst. Growth Des. 2015, 15, 3063−3075

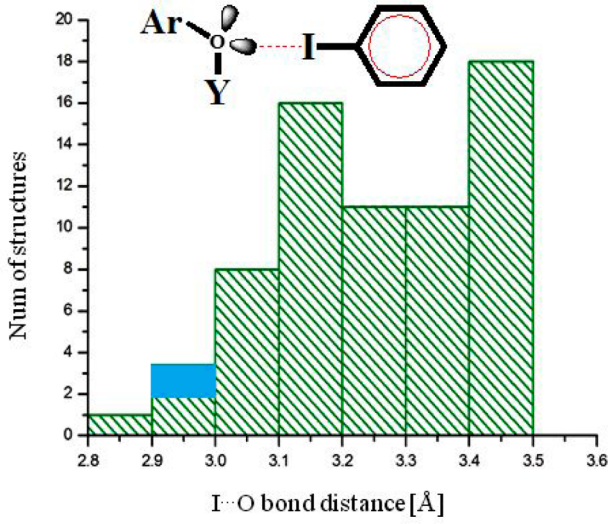

Figure 2. Histogram of crystal structures retrieved from the Cambridge Crystallographic Database exhibiting intermolecular I···O interactions between the Ar−O−Y and Ar−I fragments (see text). The blue rectangle represents the observation in compound **1**.

attempted to apply computational electrostatic considerations to these two examples by estimating the relative halogen bonding contributions. To this end we mapped the Hirshfeld surfaces[36−39] in these two structures, by using the Crystal Explorer software.[40] The Hirshfeld surface is a demonstration of the three-dimensional electron density of (electrostatic potential around) a molecule in a crystal, which is helpful in visualizing intermolecular contact interactions. In this isosurface representation of electrostatic potentials (Figure 3), red spots on the Hirshfeld maps evidence the appearance of close intermolecular interactions, such as hydrogen and halogen bonds, whereas the areas without close contacts are shown as blue regions. The contribution of the noncovalent bonds (specifically the contribution of the halogen interactions) can be analyzed by 2D fingerprint plots (Figure 3). The calculations showed that interactions involving the I atom in **1** contribute about 35.6% of the total intermolecular interactions in the crystal structure. On the other hand, the total halogen interactions contribution in HIRWEM is only about 29.7%. This suggests that the I atoms in **1** are better exposed to intermolecular contacts than in HIRTEM. Then, in **1** 4.3% and 2.1% are attributable to direct I···O and I···I attractions, respectively. The tips of the spikes on the rightmost graphs in Figure 3 are located at $di + de = 3.00$ Å (where $di + de$ represents the shortest distance between atoms inside the molecular surface and outside the surface, correspondingly). This is in good agreement with the observed I···O bond in **1**. In HIRTEM, the direct I···$N_{axial\text{-}ligand}$ contacts contribute 3.0% to the total intermolecular interaction, the I-sites being also approached by the O atoms of the DMF crystallization solvent (with a minor 0.2% contribution of the I···O_{DMF} contacts). The above illustrates that the delicate balance between the various intermolecular interactions in a given crystalline form is readily affected by subtle crystal packing effects and the crystallization solvent (if present).

Compound **2** provides another interesting example of halogen-bonded assembly of porphyrin entities in crystals. Its uniqueness lies in a successful effort to construct halogen bonded arrays not only with molecular complexes of the porphyrin scaffold but also with larger units of porphyrin-based coordination oligomers and polymers.[28] Coordination aggregates of porphyrin moieties joined by noncovalent interactions are attractive model systems from the biomimetic prospective. In the present example, we synthesized a coordination porphyrin trimer by reacting the $Sn^{IV}(OH)_2$-tetra(4′-pyridyl)-porphyrin [$Sn(OH)_2$-(B_4-P)] with Zn^{II}-tetra(4′-iodophenyl)-porphyrin [Zn-(A_4-P)]. Molecule of the former is coordinated through two trans-related pyridyl arms to the zinc centers of two units of Zn-(A_4-P) (at Zn···$N_{pyridine}$ = 2.163 Å). The trimer

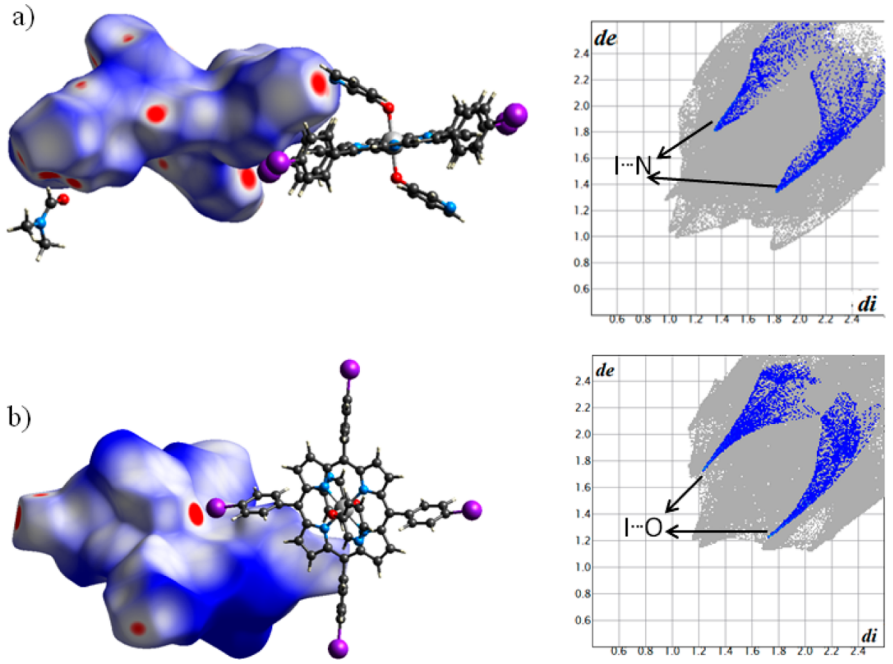

Figure 3. Calculated Hirshfeld surfaces (left) and the fingerprint plots (right) for (a) HIRWEM and (b) compound **1**. The shortest intermolecular contacts represent the I···N(axial-ligand) halogen bonds in HIRWEM, and the I···O halogen bonds in **1**.

DOI: 10.1021/acs.cgd.5b00543
Cryst. Growth Des. 2015, 15, 3063−3075

ensemble bears 4-pyridyl donor functions in the central [Sn(OH)$_2$-(B$_4$-P)] moiety and the 4-iodophenyl acceptor functions of the two peripheral five-coordinate zinc-porphyrin entities (Figure 3a). In [Sn(OH)$_2$-(B$_4$-P)], the two pyridyl groups not involved in the coordination are readily accessible as halogen bond donors for effective interaction with potential halogen bond acceptors of neighboring trimers.

Indeed, neighboring timers interact with one another via nearly linear C–I···N contacts (169.5°), forming 1D polymeric aggregates as shown in Figure 4b. The halogen bonding I···N distance is 3.193 Å, which is about 12% shorter than the sum of van der Waals radii of I and N. Tight crystal packing, bulkiness of the trimeric ensembles, and competing intermolecular interactions prevent a stronger expression of these interactions. The halogen-bonded arrays are further involved in other weak interactions, mainly contacts between hydrogen atoms and the electron-rich belt surrounding the charge-polarized I atoms, as well between the electron deficient tips of the C–I bonds and π-clouds of the aromatic residues.

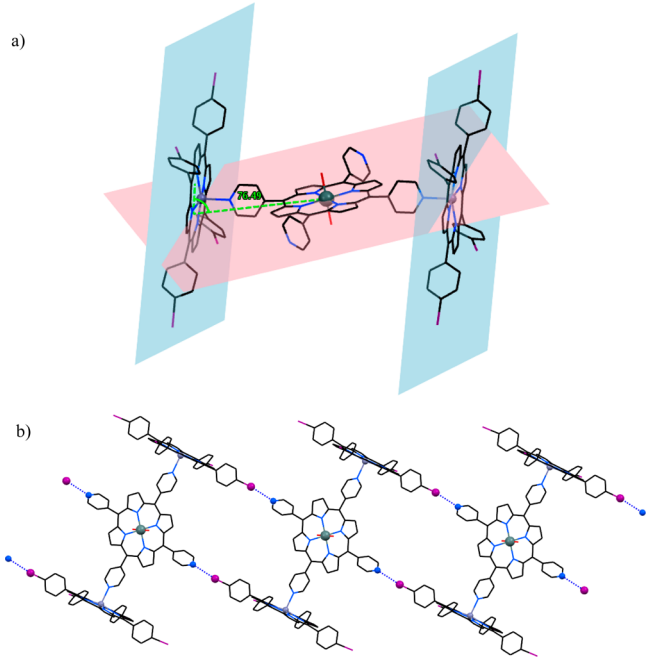

Figure 4. (a) Coordination trimer in **2**; note the tilt angle (76.5°) between the coordinating entities. (b) Halogen-bonded (dotted lines) chain of the trimer units propagating along the *b*-axis of the crystal. The metal centers as well as the interacting I (violet) and N (blue) sites are denoted by spheres.

In the next stage, it was decided to diversify the functionality of the porphyrin building units, by synthesizing molecules with mixed aryl substituents on the macrocyclic core (see in the Experimental Section for synthesis details). Thus, replacing one of the iodophenyl substituents of [Sn^{IV}(OH)$_2$-(A$_4$-P)] with a pyridyl group yielded the [Sn^{IV}(OH)$_2$-(A$_3$B-P)] scaffold, which was then utilized in the formation of **3**. The idea was to create a competition between the Lewis-base-type functions placed at the *meso* and axial position of the porphyrin and add optional sites for effective intermolecular halogen bonding. 1-Hydroxybenzotriazole was applied as an axial ligand in this case. The tin-porphyrin part in complex **3** bears three *meso*-iodophenyl arms and one pyridine substituent. The central tin ion binds to two axial ligands (tilted in the same direction with respect to the metalloporphyrin core) of deprotonated 1-hydroxybenzotriazole (Figure 5). This compound displays two possible modes of halogen bonding interactions: between the peripheral I-sites and either the *meso*-pyridine function or the triazole moiety of a neighboring porphyrin species. The first one is the pyridine ring located on the periphery of the porphyrin scaffold, and the second one comprises the N-sites of the triazole axial ligand. In **3**, the participation of the triazole in halogen interaction is hampered by the solvating DMF and water species. Then, the common mean square-planar symmetry of the porphyrin framework, combined with the asymmetric substitution pattern of the *meso*-aryl groups, results in structure **3** in a disordered distribution of the aryls around the porphyrin macrocycle. Only one (out of the four) of the disordered iodine atom positions (at site of 35% occupancy) was found to halogen bond to the pyridyl function, the observed I···N contact distance being 3.031 Å (C–I···N = 168.7°). The latter

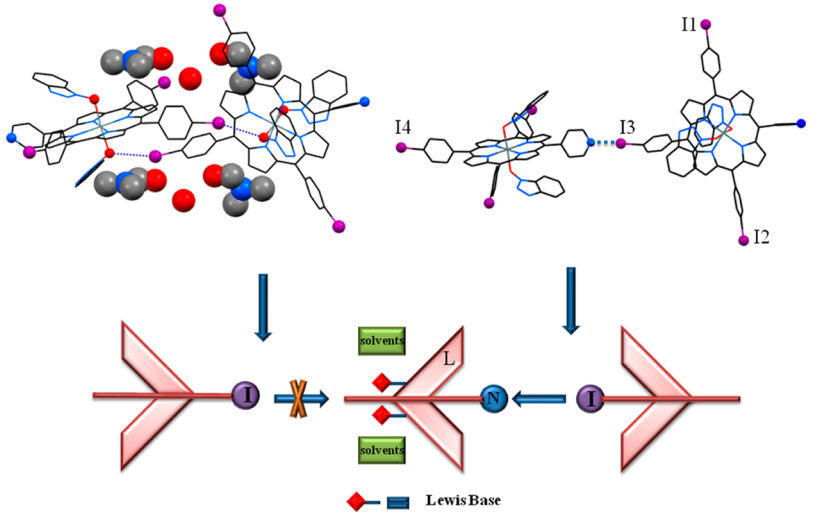

Figure 5. Schematic representation of the I···N halogen interactions (dotted lines) in **3** (only one orientation of the rotationally disordered porphyrin ring is shown). Note that an effective involvement of the triazole ligands (both inclined in the same direction with respect to the porphyrin ring) in halogen interactions with the I-sites is blocked by the DMF and water solvents (depicted by spheres in a space-filling style).

DOI: 10.1021/acs.cgd.5b00543
Cryst. Growth Des. 2015, 15, 3063–3075

is only slightly longer than the shortest interporphyrin N···I contact recorded by us earlier (2.871 Å; without activation of the aryl groups by fluorine substituents).[30] Additional halogen-type intermolecular contacts apparent in this structure are between the trans-related I-sites of one porphyrin to the O atoms of the axial ligand of adjacent units (at 3.590 Å; a shorter approach is hampered by molecules of the DMF and water solvents that surround the axial ligands). The fourth iodine site is engaged in halogen interaction with molecules of the water solvent (at nearly van der Waals I···O distance of 3.417 Å).

Numerous efforts to formulate and reliably characterize other supramolecular architectures based on the $Sn^{IV}(L)_2$-A_3B-type porphyrin scaffold have met only partial success, due to frequent observations of positional disorder of the *meso*-substituents on the porphyrin ring, as in **3**. Most of these structures could not be resolved and refined with adequate precision, as opposed to previously reported assemblies of less crowded and well-ordered A_3B-porphyrin moieties with features of supramolecular chirality.[30,41] Subsequently our attention was drawn to the A_2B_2-type porphyrin building unit of approximate D_{2h} symmetry, that bears two pairs of *trans*-related substituents of different nature (A = 4-iodophenyl and B = 4-pyridyl; Scheme 2).

The crystal structure of the corresponding free-base porphyrin (**4**, obtained unintentionally) is illustrated in Figure 6. It reveals two types of weak intermolecular interactions

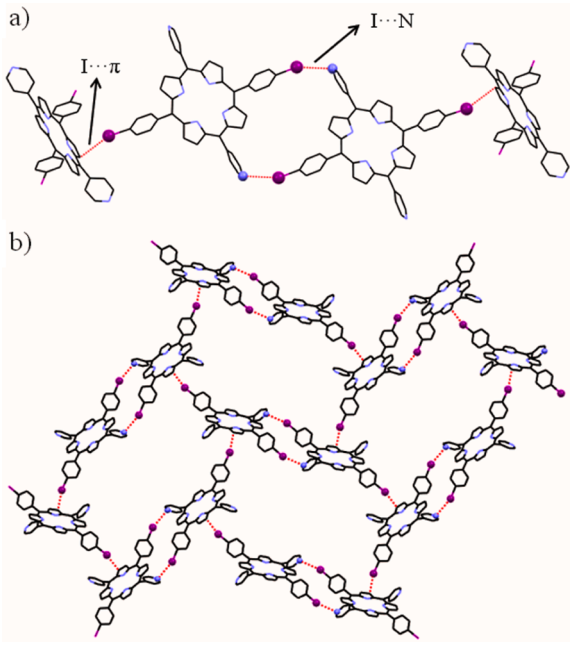

Figure 6. (a) I···N and I···π halogen interactions in **4** (marked by dotted lines). (b) The interporphyrin halogen bonded arrays aligned parallel to the (*ab*) plane of the crystal.

involving the halogen substituents: I···N contacts (at 3.378 Å) between porphyrins related by, and paired across, inversion as well as I···π (at 3.368 Å) contacts between such "dimers".[1,41,42] The resulting supramolecular arrangement represents an open 2D herringbone pattern of the porphyrin molecules criss-crossed by halogen interactions (Figure 6).

Several [$Sn(L)_2$-(A_2B_2-P)] complexes have been synthesized next with halogen- as well as hydrogen bonding capacity incorporated into the L-axial ligands. The latter variety contained N, Br, and S sites as potential halogen bond donors (to interact with the porphyrin I-sites) and -OH and -COOH substituents as hydrogen-bond donors (to interact with the pyridyl arms of the porphyrin). Along this line of reasoning, compound **5** incorporates the 5-bromopyridine-3-carboxylate anions (L4, Scheme 2) as axial ligands, and its structural features are illustrated in Figure 7. As in the previous example, the porphyrin unit (positioned in the crystal on center of inversion) exhibits approximately 73:27% positional disorder of the iodophenyl (depicted by I and I′ iodine sites, respectively) and pyridyl substituents. Apparently, the electron-withdrawing effect of the Br-substituents (which are involved in competing Br···Br contacts) on the axial ligand prevents efficient involvement of the pyridine N-sites in intermolecular I-(porphyrin)···N(axial-ligand) halogen bonding observed in earlier examples.[25]

Instead, the porphyrin complexes assemble in the form of 2D halogen-bonded networks sustained by directional I···N-(pyridyl) and I···I′ interactions (Figure 7), as shown before for the A_3B-P system.[30,41] The disordered A_2B_2-P unit imitates to some extent the overall structure of the A_3B-P framework, giving rise to similarly organized and halogen-bonding supported porphyrin ensembles. In **5**, the head-to-tail I···N distances along the *c*-axis are relatively short 3.040 and 3.091 Å, characteristic to strong halogen attractions. The σ-hole at the tip of the C−I bond is deepened in this case by simultaneous engagement of the I atoms in type-II halogen···halogen interactions (at I···I′ = 3.545 Å and C−I···I′ = 83.0°) oriented in a perpendicular direction. The Br-substituents in this structure are also involved in secondary intermolecular Br···Br contacts at 3.391 Å (C−Br···Br = 156.5°), remarkably shorter than observed recently by Bhyrappa et al. (3.472 Å) in a related porphyrinic system.[43]

In an effort to minimize the odds for rotational disorder of the porphyrin framework, it has been decided to replace the inert N-site in the axial ligand component by a more accessible carboxylic acid group of enhanced capacity to engage in lateral hydrogen as well as halogen bonding. Thus, reactions of $Sn(OH)_2$-(A_2B_2-P) with 5-bromoisophthalic acid (instead of the 3-carboxy-5-bromo-pyridine ligand) in different crystallization environments yielded two pseudopolymorphs of the corresponding Sn(5-bromoisophthalate)$_2$-porphyrin **6** (nitrobenzene solvate) and **7** (DMF solvate). As anticipated this modification changed remarkably the intermolecular binding pattern. In **6** the porphyrin complexes reside on centers of crystallographic inversion and the additional carboxylic groups (that are not coordinated to the metal center) are involved in two different types of intermolecular attraction. The carbonyl sites are engaged in linear halogen bonds with the I atoms of neighboring units of the complex at I···O = 3.015 Å and C−I···O = 175.4°. Then the −OH fragment forms a strong hydrogen bond with the *meso*-substituted pyridyl of another porphyrin moiety at O···N = 2.592 Å (Figure 8a). Thus, every porphyrin in the crystal lattice is involved in four H-bonds and four additional X-bonds with adjacent species, forming a supramolecular assembly parallel to the *ab* plane of the crystal (Figure 8b). The O···N hydrogen bonds interconnect porphyrin species displaced along the *c*-axis of the crystal, while the interporphyrin I···O halogen bonding propagates along a nearly perpendicular direction. The geometrically well-defined intermolecular interaction pattern in two dimensions effectively anchors the porphyrin framework to its neighbors in an ordered fashion. Molecules of the nitrobenzene solvate are

DOI: 10.1021/acs.cgd.5b00543
Cryst. Growth Des. 2015, 15, 3063−3075

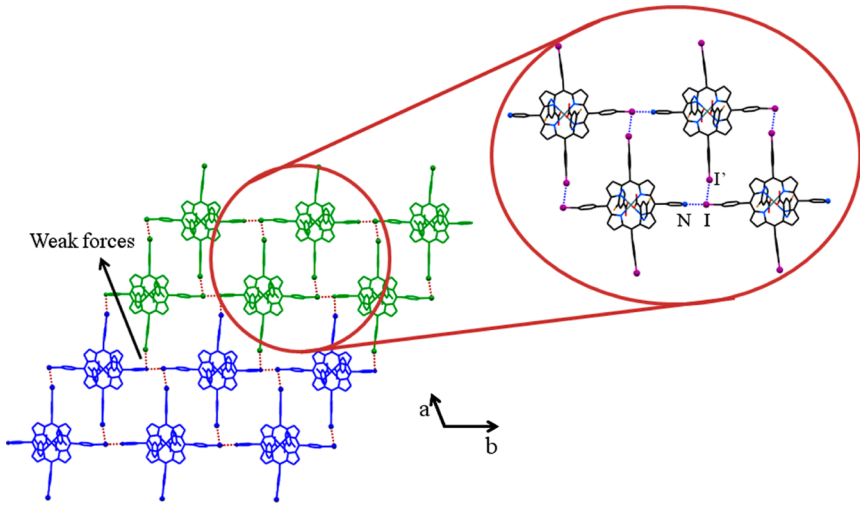

Figure 7. Illustration of the layered supramolecular arrangement of the molecular units in **5** (projection parallel to the (*ab*) plane of the crystal). The I···N and I···I′ halogen interactions that support the layered porphyrin aggregation are indicated by dotted lines.

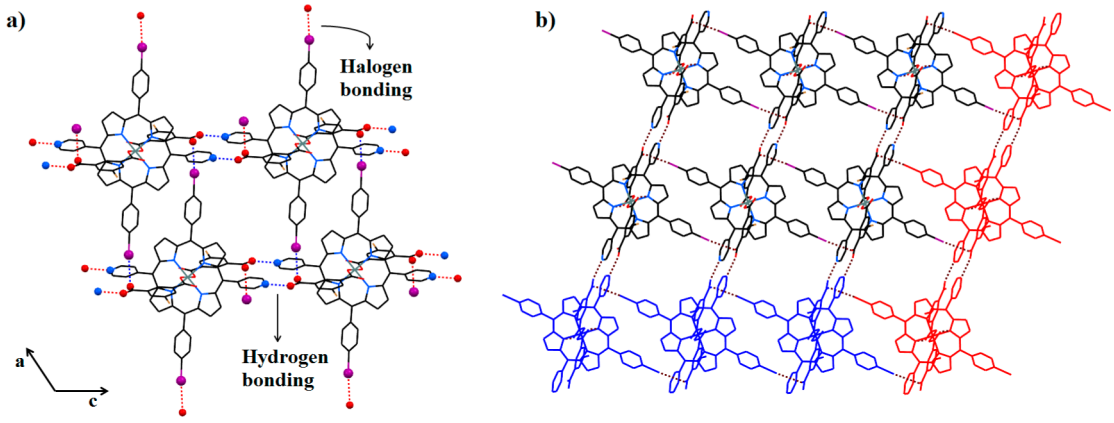

Figure 8. Illustration of (a) the strong halogen and hydrogen intermolecular interactions in **6** that extend roughly in perpendicular directions and (b) the 2D supramolecular arrays held together by the two interaction types (dotted lines). The nitrobenzene solvent is omitted for clarity. (I atoms are marked by purple spheres, O by red and N by blue spheres.)

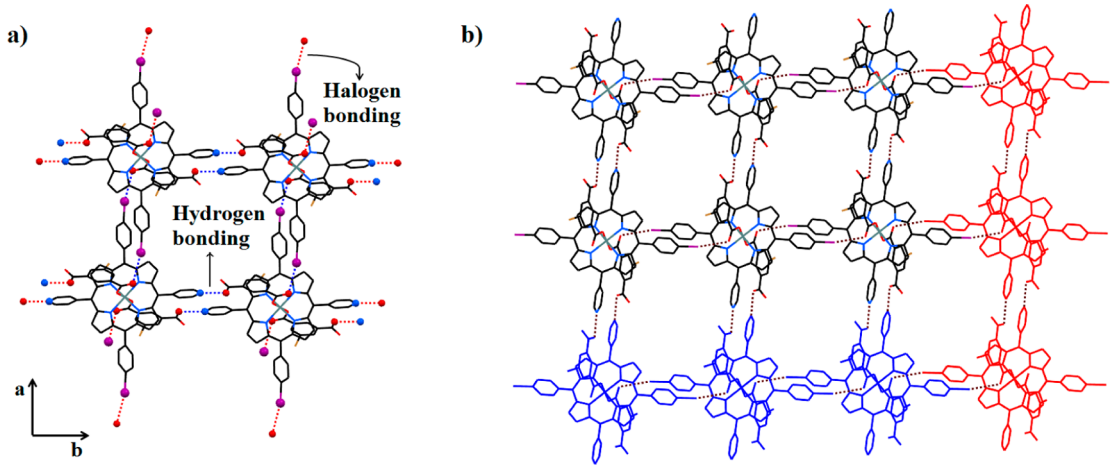

Figure 9. Layered intermolecular arrangement stabilized by a combination of hydrogen and halogen bonds (dotted lines) in **7**. In part (b) molecular units in blue are interlinked by halogen bonds, those marked in red by hydrogen bonds. The DMF solvent is omitted for clarity.

located in interstitial voids in the vicinity of the metal-coordinated carboxylate function of the ligand.

The intermolecular connectivity features in compound **7** are slightly different than in the preceding example (Figure 9). Here, the hydrogen bonding interaction from the non-coordinated carboxylic acid group to the pyridyl N-site of neighboring units is associated with proton transfer from the former to the latter. As the molecular units are located on

DOI: 10.1021/acs.cgd.5b00543
Cryst. Growth Des. 2015, 15, 3063−3075

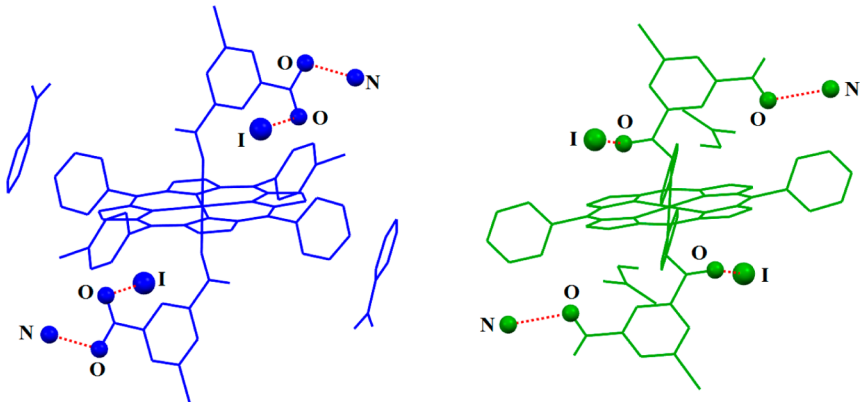

Figure 10. View of the noncovalent binding synthons in the two pseudopolymorphs between the carboxylic acid/carboxylate groups on the axial ligands and the iodophenyl and pyridyl substituents of the surrounding porphyrin entities. Compound **6** (in blue) presents two different (halogen and hydrogen bonding) perpendicularly oriented interactions of the noncoordinated carboxylic acid group, while in compound **7** (in green) both carboxylate groups are involved in intermolecular bonding.

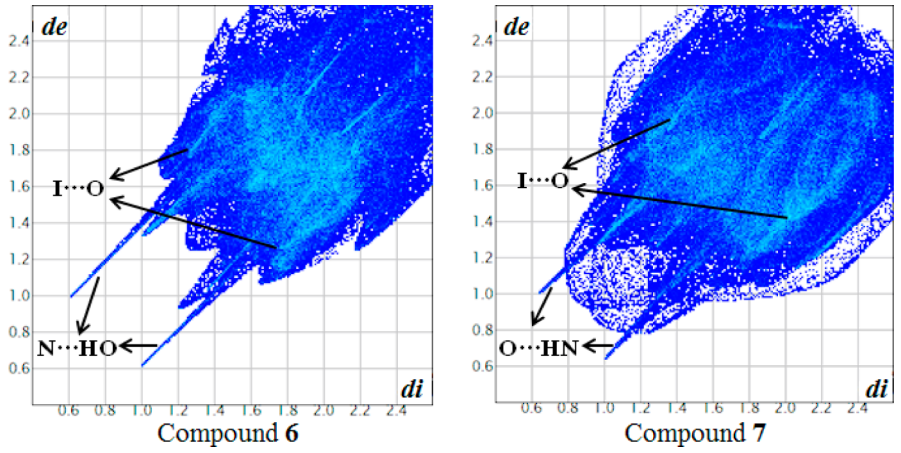

Figure 11. 2D Fingerprints of compounds **6** and **7**, exhibiting the different noncovalent interaction types. Note that the *di* + *de* values of the shown spikes correlate well with the observed interaction distances in the corresponding structures.

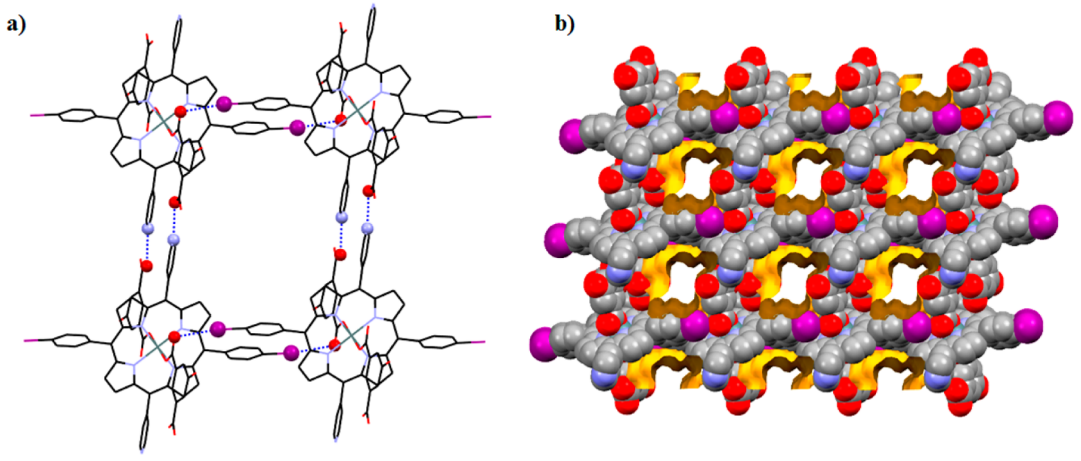

Figure 12. On the left (a), the 2D layers of compound **8** exhibit strong noncovalent interactions. On the right (b), space-filling illustration showing channel voids that consist about 25% (420 Å^3) of the crystal volume.

centers of inversion, this nearly linear interaction (at N−H···O = 2.638 Å) propagates in opposite directions, giving rise to a 1D hydrogen bonded array parallel to the *b*-axis of the crystal. Halogen bonding occurs in this structure between the 4-iodophenyl sites and the O atoms of the metal-coordinated carboxylate function. The halogen bonding in **7** (directed perpendicular to the hydrogen bonding) appears to be somewhat weaker (I···O = 3.259 Å and C−I···O = 158.4°) than in **6**, as access from neighboring units to the tin-coordinated carboxylate group is more hindered than to the one positioned on the periphery of the axial ligand. The topology of the supramolecular arrays in the two pseudo-

DOI: 10.1021/acs.cgd.5b00543
Cryst. Growth Des. 2015, 15, 3063−3075

polymorphs can be defined as 2D **sql** sheets of nearly square-planar organization in **7** and rhombohedral-like arrangement in **6**. Figure 10 provides a schematic illustration of the different intermolecular binding synthons in **6** and **7**. It shows also the relative disposition of the $PhNO_2$ and DMF solvent moieties around the porphyrin moiety.

Hirshfield calculations provide additional insight into the relative contribution of the hydrogen and halogen bonds to the total intermolecular surface−contact interactions. Interactions involving the I atom contribute 12.0% (in **6**) and 11.7% (in **7**) to the total cohesive free energy of the crystal packing; only 2.3% are attributable however to the direct I···O attractions in the two pseudopolymorphs. The minimal *de* + *di* distance between the tips of the spikes for the I···O bonds are near 3.00 Å for **6** and 3.20 Å for **7** (Figure 11), in good agreement with the observed contacts (3.016 and 3.259 Å) in the corresponding structures. The additional contribution of the specific N···O hydrogen bonding to the total energy are 2.6% in **6** ("neutral" O−H···bond) and 3.1% in **7** ("charge-assisted" $O^{-}\cdots{}^{+}HN$ bond) to the total energy. The above comparative energy estimates indicate that the two halogen and hydrogen directional interaction types have a comparable effect on the self-assembly process discussed here.

Replacement of the 5-bromoisophthalic acid (L5) by the 5-hydroxyisophthalic acid analogue (L6) as axial ligands in the reaction mixture of compound **8** led to consistent results. The structure exhibits a relatively strong intermolecular halogen interaction at I(porphyrin)···O(carboxylate) = 3.104 Å and C−I···O = 157.5°. It also reveals the presence of strong hydrogen bonding with N(porphyrin)···O(carboxylic acid) at 2.640 Å. The concerted utilization of halogen and hydrogen bonding resulted in the formation of open 2D supramolecular aggregates of **sql** topological nature (Figure 12) similar to the pattern observed in **7**. The solvent (the structure of which could not be resolved) accessible voids in this structure consist of 25.4% of the crystal volume.

The last example illustrates for the first time the occurrence of I···S halogen bonding in porphyrin assemblies, attesting to the remarkable utility of the multifunctional $[Sn(L)_2\text{-}(A_2B_2\text{-}P]$ building units in successful construction of the porphyrin supramolecular aggregates. The thiophene-dicarboxylic acid ligand (L7, Scheme 2) was used to this end. In **9** the tin center is linked from both sides of the porphyrin macrocycle to two L7 ligands. In each of these ligands the anionic carboxylate is coordinated to the tin center, while the additional carboxylic substituent and the S-site are exposed to intermolecular interaction with neighboring porphyrin entities. Indeed, the carboxylic acid functions is engaged in linear O−H···N bonds (at 2.645 Å) with the pyridyl sites of neighboring porphyrin scaffolds. The electron-rich S-sites are concurrently involved in halogen interactions with the iodophenyl ends of surrounding species at a short I···S interaction distance of 3.437 Å (C−I···S = 173.4°; the sum of van der Waals radii of I and S is approximately 3.95 Å). Each porphyrin complex is thus involved in four such I···S contacts, as well as in four hydrogen bonds. As in compounds **6**−**8**, the combination of these halogen and hydrogen interactions leads to the formation of 2D supramolecular assemblies (Figure 13), the interporphyrin voids being accommodated in the crystal by molecules of the nitrobenzene crystallization solvent.

The outcome of Hirshfield calculations (illustration of the molecular isosurface and the fingerprint plot of intermolecular contacts) in **9** is given in Figure 14. The computational results

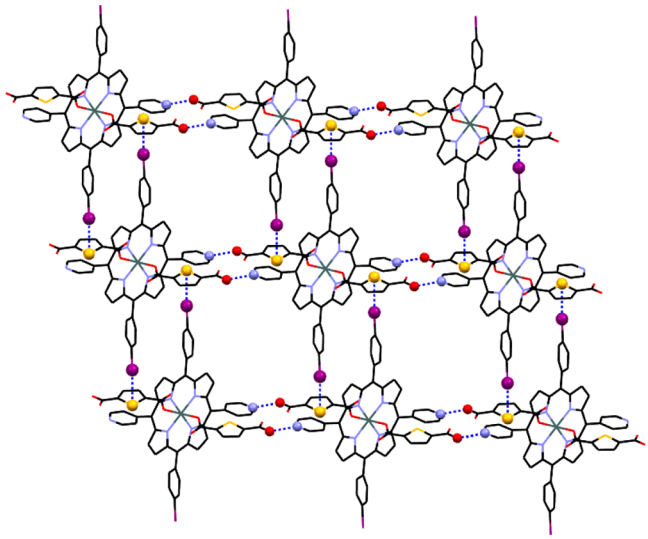

Figure 13. Compound **9** shows 2D supramolecular networking supported by I···S halogen interactions in vertical direction and N···H−O hydrogen bonds in horizontal direction. The solvent molecules are omitted for clarity. The I, N, O, and S sites, involved in these interactions are depicted by violet, blue, red, and yellow spheres, respectively.

show that the sum of intermolecular interactions contributed by the I atoms is 12.6%, but only 1.6% of these contacts is accounted for by direct but apparently weak I···S bonds. The N···H−O hydrogen bonds contribute, however, 5.7% to the total interaction energy, reflecting its dominant nature in **9** in relation to the halogen contacts.

CONCLUDING REMARKS

The above results represent new types of supramolecular porphyrin-based assemblies organized into chains or layers with the aid of halogen bonds (mainly I···O, I···N, and I···S) or a combination of halogen and hydrogen bonding interactions (OH···N/O···HN). The six-coordinate $[Sn(L)_2\text{-}(A_2B_2\text{-}P]$ porphyrin building blocks with halogen/hydrogen bond donor and acceptor functionalities placed in a complementary manner on the porphyrin framework as well as on the axial ligands (L) were found particularly useful to this end.[25,31] The multiple functionality of these units lead to the expression of cooperative directional halogen bonding in the resulting assemblies. Of particular interest in most of the presently crystal-engineered samples with carefully designed molecular scaffolds is the consistent occurrence of effective I···O halogen bonds[44] that support the formed supramolecular ensembles. A unique observation is also provided by the supramolecular aggregation of triporphyrin oligomers (as in **2**) driven by multiple I···N halogen bonds. This (along with our previous findings on similarly halogen bonded coordination polymers)[28] is possibly relevant in the context of formulations of multiporphyrin biomimetic model systems. Compounds **6**−**9** present the most attractive systems in this presentation as they reveal supramolecular assembly of the porphyrin units by concerted utilization of halogen as well as hydrogen bonding. The carefully designed and systematically varied frameworks of the $[Sn(L)_2\text{-}(A_2B_2\text{-}P)]$ type bear halogen bond donors (the B pyridyl groups) and acceptors (the A 4-iodophenyl substituents) on the porphyrin macrocycle, and halogen bond donors (N-, O-, or S-sites) placed on the axial ligands. The N-sites on

DOI: 10.1021/acs.cgd.5b00543
Cryst. Growth Des. 2015, 15, 3063−3075

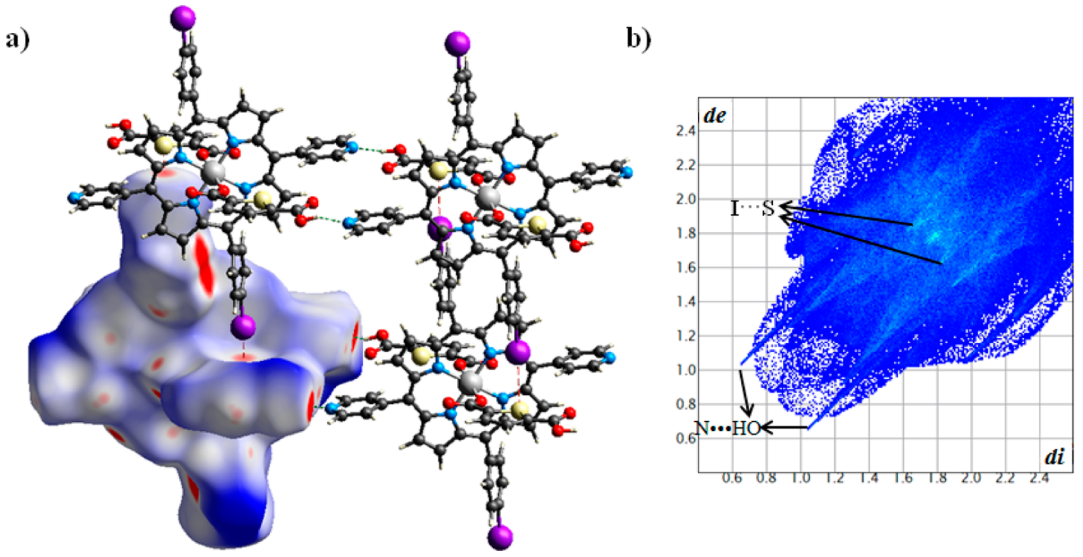

Figure 14. (a) The calculated Hirshfeld molecular surface for a fragment of **9**. (b) The 2D fingerprint plots that depict the specific I···S (halogen bond) and N···H-O (hydrogen bond) intermolecular contacts in **9**.

the porphyrin and the COOH-sites on the ligands can also act as hydrogen bond acceptors and donors, respectively, giving rise to the concerted expression of both interaction types. The resulting structures **6**–**9** consist accordingly of 2D supramolecular aggregates directed by halogen bonding in one direction and hydrogen bonding along the second dimension (each molecular unit being involved in four bonds of each type). These two specific interaction types seem to have a comparable contribution (though small) to the total cohesive energy in the corresponding structures. The relative strength of the individual forces is influenced by subtle electronic effects (i.e., activation or deactivation of the relevant binding sites by electron-donating or electron-withdrawal effects or by charge/proton transfer). Compound **9** provides an exclusive example for the first observation of I···S halogen interaction in porphyrin-based assemblies. Halogen bonds and hydrogen bonds represent weak intermolecular interactions. Yet, they can readily influence and direct the molecular self-assembly process when the building units are multiply functionalized to induce cooperative intermolecular interaction pattern of the noncovalent bonds. A better control of the supramolecular reaction environment is still required to minimize undesirable and competing effects of the crystallization solvent. The rational design of molecular structures provides an elegant approach to bottom-up fabrication of supramolecular arrays supported by directional noncovalent forces, with promising prospects in crystal engineering of new materials and practical devices whether in the bulk or on surfaces.[45]

■ ASSOCIATED CONTENT

Supporting Information

Crystallographic data for compounds **1**–**9** in the crystallographic information (CIF) format. The Supporting Information is available free of charge on the ACS Publications website at DOI: 10.1021/acs.cgd.5b00543.

■ AUTHOR INFORMATION

Corresponding Author

*E-mail: goldberg@post.tau.ac.il.

Notes

The authors declare no competing financial interest.

■ ACKNOWLEDGMENTS

This research was supported by the Israel Science Foundation (Grant No. 108/12).

■ REFERENCES

(1) Metrangolo, P.; Resnati, G.; Pilati, T.; Biella, S. In *Halogen Bonding: Fundamentals and Applications*; Metrangolo, P., Resnati, G., Eds.; Springer: Berlin, 2008; pp 105–136.
(2) Beale, T. M.; Chudzinski, M. G.; Sarwar, M. G.; Taylor, M. S. *Chem. Soc. Rev.* **2013**, *42*, 1667–1680.
(3) Parisini, E.; Metrangolo, P.; Pilati, T.; Resnati, G.; Terraneo, G. *Chem. Soc. Rev.* **2011**, *40*, 2267–2278.
(4) Metrangolo, P.; Meyer, F.; Pilati, T.; Resnati, G.; Terraneo, G. *Angew. Chem., Int. Ed.* **2008**, *47*, 6114–6127.
(5) Fourmigué, M. *Curr. Opin. Solid State Mater. Sci.* **2009**, *13*, 36–45.
(6) Bruce, D. W.; Metrangolo, P.; Meyer, F.; Prasang, C.; Resnati, G.; Terraneo, G.; Whitwood, A. C. *New J. Chem.* **2008**, *32*, 477–482.
(7) Xu, J.; Liu, X.; Lin, T.; Huang, J.; He, C. *Macromolecules* **2005**, *38*, 3554–3557.
(8) Xu, J.; Liu, X.; Ng, J. K.-P.; Lin, T.; He, C. *J. Mater. Chem.* **2006**, *16*, 3540–3545.
(9) Cariati, E.; Cavallo, G.; Forni, A.; Leem, G.; Metrangolo, P.; Meyer, F.; Resnati, G.; Righetto, S.; Terraneo, G.; Tordin, E. *Cryst. Growth Des.* **2011**, *11*, 5642–5648.
(10) Priimagi, A.; Cavallo, G.; Forni, A.; Gorynsztejn–Leben, M.; Kaivola, M.; Metrangolo, P.; Milani, R.; Shishido, A.; Pilati, T.; Resnati, G.; Terraneo, G. *Adv. Funct. Mater.* **2012**, *22*, 2572–2579.
(11) Bolton, O.; Lee, K.; Kim, H. J.; Lin, K. Y.; Kim, J. *Nat. Chem.* **2011**, *3*, 205–210.
(12) Meazza, L.; Foster, J. A.; Fucke, K.; Metrangolo, P.; Resnati, G.; Steed, J. W. *Nat. Chem.* **2013**, *5*, 42–47.
(13) Wilcken, R.; Liu, X. R.; Zimmermann, M. O.; Ruthertford, T. J.; Fersht, A. R.; Joerger, A. C.; Boeckler, F. M. *J. Am. Chem. Soc.* **2012**, *134*, 6810–6818.
(14) Walter, S. M.; Kniep, F.; Herdtweck, E.; Huber, S. M. *Angew. Chem., Int, Ed.* **2011**, *50*, 7187–7191.
(15) Coulembier, O.; Meyer, F.; Dubois, P. *Polym. Chem.* **2010**, *1*, 434–437.
(16) Mele, A.; Metrangolo, P.; Neukirch, H.; Pilati, T.; Resnati, G. *J. Am. Chem. Soc.* **2005**, *127*, 14972–14973.

DOI: 10.1021/acs.cgd.5b00543
Cryst. Growth Des. 2015, 15, 3063–3075

(17) Rissanen, K. *CrystEngComm* **2008**, *10*, 1107−1113.
(18) Choi, E.-Y.; Barron, P. M.; Novotney, R. W.; Hu, C.; Kwon, Y.-UK; Choe, W. *CrystEngComm* **2008**, *10*, 824−826.
(19) Fujiwara, K.; Kurahashi, T.; Matsubara, S. *J. Am. Chem. Soc.* **2012**, *134*, 5512−5515.
(20) Schuckman, A. E.; Batteas, J. D.; Drain, C. M. *Coord. Chem. Rev.* **2010**, *254*, 2297−2310.
(21) Goldberg, I. *Chem.—Eur. J.* **2000**, *6*, 3863−3870.
(22) Goldberg, I. *Chem. Commun.* **2005**, 1243−1254.
(23) Goldberg, I. *CrystEngComm* **2008**, *10*, 637−645.
(24) Syssa-Magalé, J.-L.; Boubekeur, K.; Leroy, J.; Chamoreau, L.-M.; Fave, C.; Schöllhorn, B. *CrystEngComm* **2014**, *16*, 10380−10384.
(25) Titi, H. M.; Patra, R.; Goldberg, I. *Chem.—Eur. J.* **2013**, *19*, 14941−14949.
(26) Nandi, G.; Titi, H. M.; Goldberg, I. *Cryst. Growth Des.* **2014**, *14*, 3557−3566.
(27) Titi, H. M.; Patra, R.; Goldberg, I. *Acta Crystallogr., Sect. C* **2013**, *69*, 1013−1016.
(28) Nandi, G.; Goldberg, I. *CrystEngComm* **2014**, *16*, 8327−8333.
(29) Titi, H. M.; Karmakar, A.; Goldberg, I. *J. Porphyrins Phthalocyanines* **2011**, *15*, 1250−1257.
(30) Muniappan, S.; Lipstman, S.; Goldberg, I. *Chem. Commun.* **2008**, 1777−1779.
(31) Patra, R.; Titi, H. M.; Goldberg, I. *Cryst. Growth Des.* **2013**, *13*, 1342−1349.
(32) Boccalon, M.; Iengo, E.; Tecilla, P. *J. Am. Chem. Soc.* **2012**, *134*, 20310−20313.
(33) Sheldrick, G. M. *Acta Crystallogr., Sect. A: Found. Crystallogr.* **2015**, *71*, 3−8.
(34) Sheldrick, G. M. *Acta Crystallogr., Sect. C: Struct. Chem.* **2015**, *71*, 3−8.
(35) Spek, A. L. *Acta Crystallogr., Sect. C: Struct. Chem.* **2015**, *71*, 9−18.
(36) Spackman, M. A.; Jayatilaka, D. *CrystEngComm* **2009**, *11*, 19−32.
(37) Spackman, M. A.; McKinnon, J. J. *CrystEngComm* **2002**, *4*, 378−392.
(38) Wang, R.; Dols, T. S.; Lehmann, C. W.; Englert, U. *Chem. Commun.* **2012**, *48*, 6830−6832.
(39) McKinnon, J. J.; Jayatilaka, D.; Spackman, M. A. *Chem. Commun.* **2007**, 3814−3816.
(40) *CrystalExplorer 2.1*; Wolff, S. K.; Grimwood, D. J.; McKinnon, J. J.; Jayatilaka, D.; Spackman, M. A. University of Western Australia: Crawley, Western Australia, 2007; http://hirshfeldsurface.net.
(41) Lipstman, S.; Muniappan, S.; Goldberg, I. *Cryst. Growth Des.* **2008**, *8*, 1682−1688.
(42) Adams, C. J.; Bowen, L. E. *Dalton Trans.* **2005**, 2239−2240.
(43) Bhyrappa, P.; Purushothaman, B.; Vittal, J. J. *J. Porphyrins Phthalocyanines* **2003**, *7*, 682−692.
(44) Gavezzotti, A. *J. Am. Chem. Soc.* **1983**, *105*, 5220−5225.
(45) Mukherjee, A.; Tothadi, S.; Desiraju, R. *Acc. Chem. Res.* **2014**, *47*, 2514−2524.

DOI: 10.1021/acs.cgd.5b00543
Cryst. Growth Des. 2015, 15, 3063−3075